

GA-A25943

EDGE STABILITY OF STATIONARY ELM-SUPPRESSED REGIMES ON DIII-D

by

T.H. OSBORNE, P.B. SNYDER, K.H. BURRELL, T.E. EVANS,
M.E. FENSTERMACHER, A.W. LEONARD, R.A. MOYER,
M.J. SCHAFFER, AND W.P. WEST

SEPTEMBER 2007



DISCLAIMER

This report was prepared as an account of work sponsored by an agency of the United States Government. Neither the United States Government nor any agency thereof, nor any of their employees, makes any warranty, express or implied, or assumes any legal liability or responsibility for the accuracy, completeness, or usefulness of any information, apparatus, product, or process disclosed, or represents that its use would not infringe privately owned rights. Reference herein to any specific commercial product, process, or service by trade name, trademark, manufacturer, or otherwise, does not necessarily constitute or imply its endorsement, recommendation, or favoring by the United States Government or any agency thereof. The views and opinions of authors expressed herein do not necessarily state or reflect those of the United States Government or any agency thereof.

EDGE STABILITY OF STATIONARY ELM-SUPPRESSED REGIMES ON DIII-D

by

T.H. OSBORNE, P.B. SNYDER, K.H. BURRELL, T.E. EVANS,
M.E. FENSTERMACHER,* A.W. LEONARD, R.A. MOYER,†
M.J. SCHAFFER, AND W.P. WEST

*Lawrence Livermore National Laboratory, Livermore, California

†University of California San Diego, La Jolla, California

This is a preprint of a paper to be presented at the 11th IAEA Technical Meeting on H-Mode Physics and Transport Barriers, in Tsukuba, Japan on September 26-28, 2007 and to be published in the *Proceedings*.

Work supported by
the U.S. Department of Energy
under DE-FC02-04ER54698, W-7405-ENG-48,
DE-FG02-04ER54758

GENERAL ATOMICS PROJECT 30200
SEPTEMBER 2007

ABSTRACT

We discuss the MHD stability of the H-mode pedestal region in two edge localized mode (ELM)-suppressed H-mode regimes on DIII-D, the quiescent (QH)-mode and resonant magnetic perturbation (RMP) H-mode. The QH-mode is obtained at low density with most of the neutral beam power injected counter to the plasma current, and is characterized by a continuous, low toroidal mode number (n), edge harmonic oscillation (EHO). QH-mode is observed to transition back to ELMing H-mode as the rotational shear is decreased by increasing the co-current neutral beam power fraction or by increasing the plasma to conducting wall distance, consistent with a model for the EHO as a peeling instability with added drive from rotational shear, which saturates through self transport of momentum or damping of rotation through drag of the mode on the conducting wall. In RMP H-mode, an $n=3$ coil provides the non-axisymmetric perturbation. Two regimes of RMP ELM suppression are observed. At low collisionality with large resonant field perturbation, the pedestal pressure gradient and current density are reduced below the peeling-ballooning mode stability limit; while at higher collisionality with large non-resonant perturbation there is little change in the pedestal parameters and type II ELMs are enhanced.

1. INTRODUCTION

The two principal large scale instabilities in the H-mode edge transport barrier (ETB) are the pressure gradient, p' , driven ballooning mode and the current density, J , driven peeling mode. At ratios of p'/J common in experiments, the most unstable mode has both peeling and ballooning characteristics. The theory of the peeling-ballooning mode is well established [1] and there is strong experimental support that this instability sets the threshold for the onset of the ELM [2,3]. When ideal MHD is extended with two-fluid theory, it is found that diamagnetic effects can have a strong impact on the mode growth rate [4]. The mode growth rate remains relatively constant when diamagnetic effects are weak, $\omega_{*i} < 2\gamma_0$, where γ_0 is the growth rate computed without two fluid effects, and the ion diamagnetic frequency is given by $\omega_{*i} = (nT_i/en_i)(\partial n_i/\partial\Psi)$, where n is the toroidal mode number, T_i is the ion temperature, n_i is the ion density, and Ψ is the MHD poloidal flux. When diamagnetic effects are strong, $\omega_{*i} > 2\gamma_0$, the growth rate of the mode is strongly reduced, so that $\gamma_0/(\omega_{*i}/2) = 1$ sets a threshold for instability (Fig. 1). The variation of the toroidal mode number along the $\gamma/(\omega_{*i}/2) = 1$ stability threshold plays a role in the interpretation our results. For these experiments $n \approx 10$ where peeling and ballooning mode branches merge, and n decreases as the modes become more peeling-like and J driven, while n increases as the modes become more ballooning-like and p' driven. ELMs are observed when the equilibrium point reaches either the J or p' dominated boundaries. The current density in the ETB is predominantly bootstrap current, which is proportional to p' , but also decreases with increasing collisionality, ν_* [5]. Increasing ν_* in the ETB, for example by raising the density, then moves the equilibrium from the low- n , J driven boundary to the intermediate- n , p' driven boundary. Such a variation of ELM precursor mode number with density is observed experimentally [6].

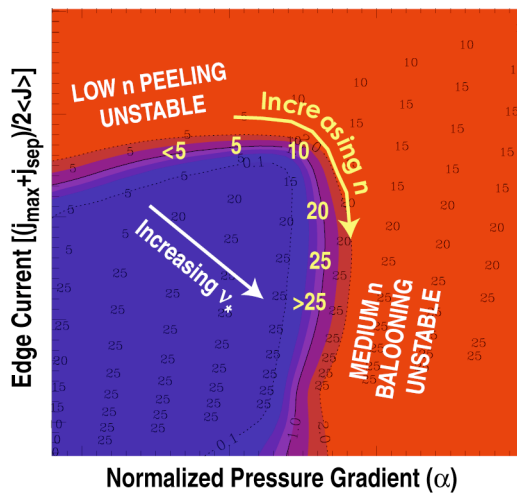


Fig. 1. Peeling-ballooning mode stability diagram. Contours of growth rate over $1/2$ ion diamagnetic frequency as a function of normalized pressure gradient and normalized current density. $\gamma/(\omega_{*i}/2) = 1$ separates the stable (blue) from unstable region (red). Toroidal mode number, n , of most unstable mode increases in going from current to pressure gradient driven boundaries. Increasing collisionality, ν_* , reduces j -bootstrap favoring higher n .

On DIII-D two ELM-suppressed H-mode regimes, the quiescent or QH-mode [7], and the H-mode with resonant magnetic perturbation (RMP) H-mode [8] are under study. In these regimes the undesirable bursts of enhanced transport accompanying the ELMs are replaced by a continuous loss. In the case of QH-mode, evidence is presented which suggests that an additional drive mechanism, toroidal rotational shear, coupled with a rotational damping mechanism, such as wall drag, leads to saturation of modes at low n before the current density can reach the level required to trigger an ELM. In this case the saturated peeling-ballooning mode itself provides the transport necessary to avoid the ELM. In the case of the RMP H-mode, an externally applied helical magnetic field, which is expected to break up the magnetic surfaces in the ETB region, directly provides the transport required to keep the edge p' and J below the ELM instability threshold [8].

2. EXPERIMENTAL METHOD

The pressure profiles used for the stability analysis are determined experimentally as the sum of the electron pressure, the deuteron pressure, the pressure of fully stripped carbon (which is the only significant impurity in DIII-D), the fast ion pressure computed using the NFREYA module of the ONETWO transport code [9], and the lowest order contribution of the rotational energy to the pressure. The extent of the edge steep gradient region of the electron profiles on the outboard midplane is 1 to 2 cm, while it is somewhat wider, 1.5 to 3 cm, for the ion profiles. The electron pressure is determined using the DIII-D multi-pulse Thomson scattering system which measures the electron density and temperature at 37 points along a vertical chord every 12.5 ms. When mapped to the outboard midplane, the spatial resolution of the Thomson scattering system is about 0.6 cm in the ETB region. The ion temperature, C^{6+} density, and rotational speed for C^{6+} ions are measured with the DIII-D charge exchange recombination spectroscopy system (CER) that has 0.5 cm spatial resolution in the ETB region and can be run at up to 0.274 ms time resolution. The deuteron density is computed from the electron density, the fast ion density, and the C^{6+} density, assuming C^{6+} is the only impurity. The fast ion and rotational pressures are generally small in the ETB.

Profile data is averaged over a steady state phase of a discharge, or from a particular phase of the inter-ELM period for many similar ELMs, by combining profiles as a function of poloidal flux based on equilibrium, computed at the individual times of the profile measurements. By mapping to a temporally local equilibrium, small sweeps in the separatrix location can be used to improve the effective experimental radial point density in the ETB. The absolute location of the electron profiles relative to the separatrix has significant uncertainty due to the sensitivity of the equilibrium to uncertainties in the magnetics measurements. UEDGE divertor modeling simulations of a number of DIII-D discharges result in T_e profiles which are well represented by a hyperbolic tangent form with the separatrix located at one-half the width of the hyperbolic tangent outside of its inflection point [10]. This prescription was used to locate the separatrix relative to the averaged n_e and T_e profiles.

Equilibria used for stability analysis were generated with the EFIT code [11] with the pressure profile set as described above. The current density profile in the core plasma is determined from motional stark effect (MSE) measurements. The MSE system cannot be used to determine the current density profile in the ETB due to the large static electric field in this region. A lithium beam probe system, based instead on Zeeman splitting, has been used to measure the current density profile in the ETB for a limited number of discharges. These measurements indicate that the current density profile in the ETB is in good agreement with the neoclassical value [12]. Therefore, for the stability analysis that follows, the neoclassical value given by Sauter [5] for the bootstrap current is assumed.

3. ELITE STABILITY CALCULATIONS

The ELITE code [13] is used for the ETB stability calculations. ELITE is a 2D, linear, eigenvalue code based on ideal magnetohydrodynamic (MHD) utilizing a generalization of ballooning mode theory that makes use of poloidal harmonic localization to achieve high efficiency. ELITE computes the growth rates for a spectrum of modes with different toroidal mode numbers covering the range of n values of importance in the ETB. The eigenfunction of the peeling-ballooning instability at a given n number generally covers the entire ETB region, combining a range of poloidal mode numbers rather than being characteristic of a single rational surface. After computing the stability, $\gamma/(\omega_{*i}/2)$, of the experimental equilibrium, variations of J and p' in the ETB of this equilibrium are made and $\gamma/(\omega_{*i}/2)$ is recomputed to map out the stability boundary (Fig. 1).

4. QH-MODE

QH-mode [7] is an ELM-suppressed regime of high energy confinement with constant density and radiated power. It requires operation at low density or collisionality [5], $v_e^* \sim 0.1$, and injection of at least 80% of the neutral beams in the toroidal direction opposite to the direction of the plasma current. QH-mode is generally accompanied by the edge harmonic oscillation (EHO), which is observed on magnetic probes as a series of low- n harmonics with typically $n=1$ to 4 the dominant component. When the EHO is not present, as for example when the power is reduced below the power threshold, the discharge returns to standard ELM-free H-mode and the density rapidly rises, suggesting that the EHO provides the particle transport to keep QH-mode in steady state. Similar enhancements in impurity and momentum transport are also associated with the EHO [14].

4.1. QH-mode Edge Stability

Evaluation of the peeling-ballooning stability for discharges covering a range of cross-sectional shapes shows that the QH-mode edge is always near the low toroidal mode number, $n \leq 5$, peeling mode instability boundary (Fig. 2). This association with low- n instability suggests a connection between the EHO and the peeling-ballooning mode. The existence of an upper density operational limit suggests that low- n peeling mode instability may be a required feature of QH-mode. Increasing the density increases the collisionality for a given H-mode pedestal pressure, $v_*^{PED} \propto (n^{PED})^3 / (p^{PED})^2$, which suppresses the bootstrap current and shifts the instability point toward the high- n ballooning mode branch (Fig. 1). At fixed collisionality $n^{PED} \propto (p^{PED})^{2/3}$, so that stronger plasma shaping, which raises the peeling-ballooning mode stability limit (Fig. 2) should allow higher density operation. This was verified in experiments in which the QH-mode density limit doubled as the triangularity was increased from 0.65 to 0.85. At the higher triangularity in this experiment the density in QH-mode was as high as typical H-mode discharges with ELMs, $n_e^{PED} / n_{Greenwald} = 0.5$, where $n_{Greenwald} (10^{20} m^{-3}) = I_P (MA) / \pi a (m)^2$ [22]. ELITE modeling confirms that it is possible to reach a higher density while maintaining access to the low- n peeling mode unstable regime at higher triangularity [16].

The proximity of the QH-mode edge to the low- n peeling stability boundary suggests the EHO may represent a saturated state of this instability. Observation of density fluctuations using beam emission spectroscopy on DIII-D showed the EHO to be localized to the ETB region, and that there are no phase inversions that would suggest a non-ideal mode [14]. Further evidence that the EHO is associated with the current driven peeling boundary is given by current ramp experiments [15], where a downward current ramp turned off the EHO, while an upward current ramp triggered ELMs. This result indicates not only that the EHO is current driven, but also that it is destabilized at currents below those that would be required to trigger an ELM. Further evidence of this relationship between the EHO and ELM stability

limits comes from a series of discharges in which the fraction of neutral beam power in the direction of plasma current was increased until ELMs were triggered, while keeping the total power input and other characteristics of the discharge fixed. Stability analysis of these discharges shows that the cases with ELMs lie very close to the low- n peeling mode stability limit while the QH-mode discharges with the EHO are situated somewhat below this limit (Fig. 3).

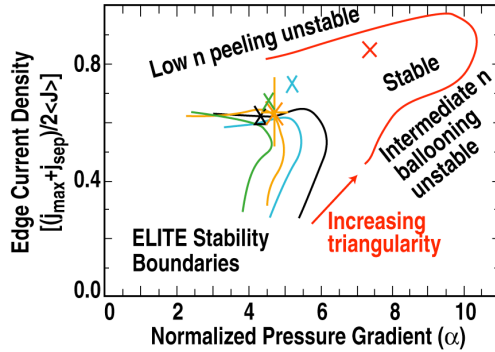


Fig. 2. Peeling-ballooning mode stability boundaries for different QH-mode discharge shapes (lines) shows that the operational point for the ETB (Xs) always lies near the low- n peeling unstable boundary.

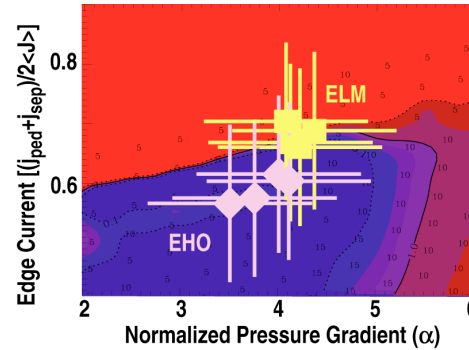


Fig. 3. Discharges with small co-NBI power (diamonds) are in QH-mode with EHO and further in the stable region (dark blue) than discharges with large co-NBI (squares) where ELMs appear.

4.2. Rotational Shear and QH-mode

Toroidal rotational shear may provide the additional instability drive to trigger the EHO at edge currents below what would be required for the purely current driven peeling mode. ELITE modeling indicates that while rotational shear is stabilizing for modes at intermediate to higher toroidal mode number, it is destabilizing for modes at low- n [16]. Saturation of the instability might occur through self transport of momentum or drag of the mode on the conducting wall. The rotational shear is clearly reduced in the presence of the EHO. In the current ramp-down experiment described above for example, when the EHO is switched off the rotational shear rapidly increases.

Previous results indicated that the rotational shear in the ETB is significantly higher in QH-mode with counter-injection compared to ELMing H-mode discharges with pure co-injection at the same density [17]. Since the rotational shear is reduced in the presence of the EHO, this implies that high rotational shear is a property of counter-injection in general, and may explain why counter-injection is required for QH-mode. Low density operation would also increase the rotation speed by reducing the plasma inertia.

The importance of rotational shear was verified in an experiment where the rotational shear was varied by varying the fraction of neutral beam power (NBI) in the co-current direction. In this experiment the NBI was switched from pure counter to some fraction co-current after QH-mode was obtained, keeping the total heating power fixed. As the co-NBI

fraction increased the rotational shear decreased. The initially $n = 3$ dominant EHO turned off progressively earlier as the co-NBI fraction was increased. Below co-NBI fractions of 20% the EHO returned intermittently as $n = 1$ or $n = 2$. Above 20% co-NBI, ELMs appeared, with ELMs coming sooner in discharges with higher co-NBI power fraction. Once the ELMs began, the rotational shear was reduced to near zero and the EHO did not reappear. The pressure gradient and current density also increased as the co-NBI fraction increased. This increase in the pedestal pressure came primarily through an increase in the pedestal density and expansion of the steep gradient region of the density inwards which began with the start of co-NBI. In the higher co-NBI fraction cases where ELMs returned, the primary $n = 3$ EHO turned off a few 100 ms before the first ELM. In some cases the first ELM then occurred with no EHO present, but in others the EHO returned initially as $n = 2$, then switched to $n = 1$ and subsequently grew to large amplitude over a few ms time scale as a precursor to the ELM.

The importance of drag of the mode on the conducting wall as a factor in EHO saturation was consistent with results from an experiment in which the distance between the vessel wall and the plasma was varied in QH-mode. In this experiment, the EHO was switched off and ELMs returned as the plasma-wall separation at the outboard midplane was increased from 12 to 19 cm. The ETB pressure and current density profiles were similar at these two plasma-wall separation values, and ELITE analysis indicates both lie at the low- n peeling instability threshold within experimental uncertainties. The rotational shear was found to be larger in the discharge with small plasma-wall separation [Fig. 4(a)]. ELITE analysis of the small plasma-wall separation discharge shows that rotational shear is destabilizing as expected, and that the peak growth rate occurs at $n = 5$ consistent with the dominant EHO harmonic [Fig. 4(b)].

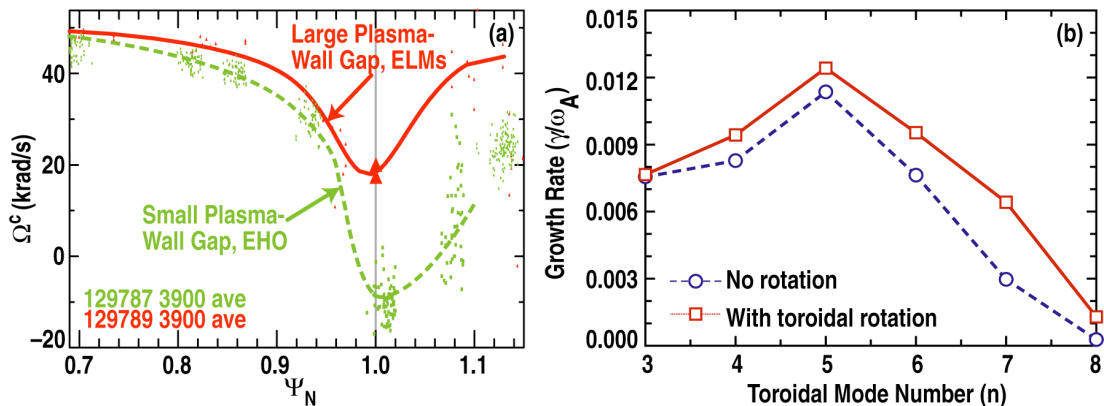


Fig. 4. (a) Angular toroidal rotation velocity for carbon ions versus normalized poloidal flux. Discharge with small plasma-wall gap (green-dash) has larger rotational shear in ETB region, $0.9 < \psi_N < 1.0$, compared to larger plasma-wall gap discharge (red). (b) ELITE stability calculation of growth rate versus toroidal mode number for small plasma-wall gap discharge [green in (a)], showing rotational shear (green) increases growth rate relative to no rotation case (black-dash). Growth rate peaks at $n = 5$ in agreement with observed EHO primary mode number.

5. RMP H-MODE

As has been previously reported [18] the DIII-D resonant magnetic perturbation, RMP, coil is effective at suppressing ELMs. The DIII-D RMP coil is composed of two coil sets located symmetrically above and below the vessel midplane on the large major radius side. Each coil set is made up of six coils where toroidally adjacent coils are connected to carry equal and opposite currents producing an $n = 3$ perturbation.

The RMP coil was effective at eliminating ELMs in low collisionality, $\nu_e^* \sim 0.1$, discharges, with the coil configured to produce the maximum field perturbation resonant with the equilibrium field. This configuration is expected to induce the largest magnetic islands in the ETB, giving regions of stochastic field and enhanced transport with the goal of controlling the pedestal pressure and thereby avoiding the peeling-ballooning instability. Resonance and ELM suppression is achieved with the upper and lower coil sets mirroring each other (even parity) when the discharge safety factor at the 95% flux surface, $q_{95} \approx 3.7$. In this regime both large Type I ELMs and small Type II ELMs are eliminated. An odd parity coil connection is not effective at suppressing ELMs at $q_{95} \approx 3.7$ and $\nu_e^* \sim 0.1$. Resonance is also achieved at $q_{95} \approx 7.5$ with the current in the upper and lower coil sets rotated 60° with respect to each other, odd parity. In this case, ELMs are strongly reduced in amplitude. In both the $q_{95} \approx 3.7$ and 7.5 cases, significant effects on the H-mode pedestal are observed [18].

RMP ELM suppression also occurred at $\nu_e^* \sim 1$, and $q_{95} \approx 3.7$ with the RMP coils in odd parity. Under these conditions, the resonant part of the field is reduced by roughly a factor of 7 compared to an even parity connection for the same coil current, although the total field from the coil in the ETB is comparable. In this case there is very little effect on the ETB pressure profile and, although Type I ELMs can be completely eliminated, small Type II ELMs are enhanced in amplitude.

5.1. RMP H-mode at $\nu_e^* \sim 0.1$, $q_{95} \approx 3.7$, Even RMP Coil Parity

Previous results in low triangularity, $\delta = 0.5(\delta_{UPPER} + \delta_{LOWER}) = 0.26$, discharges have shown that at $\nu_e^* \sim 0.1$ the RMP suppresses ELMs by reducing the pressure gradient and current density in the ETB below the peeling-ballooning mode stability threshold [18]. That effect is confirmed here for discharges with ITER similar cross-sectional shapes at average triangularity $\delta = 0.53$ [Fig. 5(a)]. The pressure gradient and current density limits in the higher triangularity, ITER similar shape, discharges were however, unexpectedly, reduced. This reduction in the instability threshold may be driven by an unexplained expansion in the ETB width in the ITER similar shape discharges compared to the lower triangularity discharges [Fig. 5(b)]. ELITE modeling results for the ITER similar shape indicate the pressure gradient limit is reduced when the ETB pressure width, Δ , expands as $p'_{CRIT} \propto \Delta^{-0.25}$

consistent with previous results for $\delta=0$ [2]. This effect is a result of shifting the pressure gradient and current peaks outwards to more strongly shaped surfaces as Δ is reduced and from improved stability of the more radially extended lower n modes. The reduction in stability limit and expansion in width of the ETB in the higher triangularity, ITER similar shape discharges are offsetting so that similar pedestal pressure was obtained in these discharges compared to previous results at lower triangularity. At the minimum RMP coil current required for ELM suppression, the pedestal pressure for both the low and high triangularity cases was about 60 % of the peak pedestal pressure before an ELM without the RMP, and about 80% of the pedestal pressure when averaged over ELMs. The main effect of the RMP is to reduce the pedestal electron density for both the low and high triangularity shapes. There is also a narrowing of the steep gradient region for the electron profiles. Despite the reduction in pedestal pressure there was little change in the overall energy confinement enhancement factor in RMP ELM suppressed discharges, as a result of some peaking of the density profile and increase in the ion temperature.

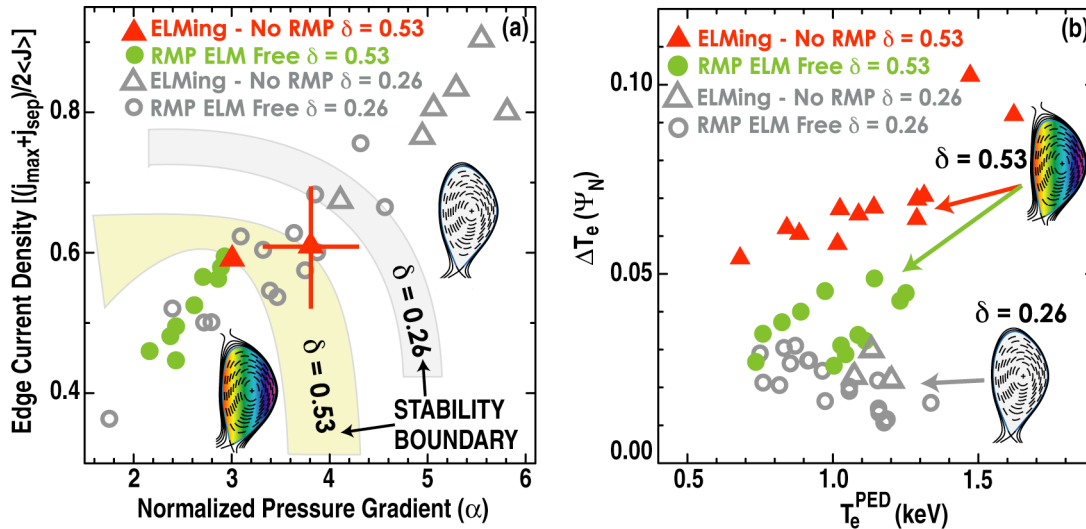


Fig. 5. (a) Peeling-ballooning instability boundaries and data points for triangularities $\delta = 0.26$ (open points), and $\delta = 0.53$ (filled points) for RMP ELM free (circles) and no-RMP ELMing discharge (triangles). (b) ETB width (width of steep gradient region in T_e) is larger at $\delta = 0.53$ (filled points) compared to $\delta = 0.26$ data (open points).

As discussed in section 2, the location of the foot of the electron temperature profile relative to the separatrix has significant uncertainty. In discharges with the RMP, one might expect a region of stochastic field and hence low pressure gradient to exist just within the separatrix. To investigate the effect of such a region on stability, ELITE analysis was carried out with the electron profiles shifted inward relative to the separatrix. If the vacuum region, outside of which $j=0$ in the ELITE calculation, is maintained at the original separatrix, equivalent to assuming that the stochastic region is filled with low pressure plasma, this has a strong stabilizing effect on the peeling modes as a result of moving the ETB current density

away from the plasma boundary. If instead the plasma boundary is also shifted inwards, equivalent to treating the stochastic region as vacuum, both the peeling and ballooning modes become more unstable as a result of the shift of the pressure gradient and current density to less strongly shaped surfaces.

Increasing density with gas puffing in RMP ELM suppressed discharges raised the pedestal density and pressure and brought back the ELMs. At first the ELMs were small and high frequency but they became larger as the density was increased. The reappearance of ELMs is consistent with stability analysis which indicated the pressure gradient reached the ballooning limit with $n \sim 25 - 30$. If the RMP coil is switched off after the density rise, the ELMs become much larger and less frequent, the pedestal expands, and the most unstable mode is computed to have $n \sim 15$.

5.2. RMP H-mode at $v_e^* \sim 1$, $q_{95} \approx 3.7$, Odd RMP Coil Parity

Even though the resonant magnetic field perturbation is small in the case of odd RMP coil parity at $q_{95} \approx 3.7$, complete Type I ELM suppression was achieved with this configuration in $v_e^* \sim 1$, higher triangularity discharges. When the ELMs were suppressed, the H-mode energy confinement enhancement factor remained unchanged. The electron density, n_e , electron temperature, T_e , and ion temperature profiles, T_i , also changed very little, both overall and in the pedestal region, in the RMP coil ELM suppressed phase compared to the ELMing case with no-RMP (Fig. 6). There was typically some rise in the effective charge, Z_{eff} , across the profile with the RMP coil on. The toroidal rotation speed measured for the carbon impurity, Ω_ϕ^C , is dramatically reduced with the RMP coil on over the entire plasma cross-section. No cases were observed for which the total pressure, P_{TOT} , in the pedestal region in the RMP coil ELM suppressed phase was significantly different from the profile before a Type I ELM with the RMP coil off under otherwise similar discharge conditions. As would be expected from the similar pedestal pressure profiles with and without the RMP coil, peeling-ballooning mode stability calculations give similar growth rates and toroidal mode numbers. In cases where the Type I ELMs were only reduced in frequency rather than being completely suppressed, the energy loss and profile change associated with the Type I ELMs, and the magnetic fluctuations at the ELM were similar with the RMP coil on and off.

A typical feature of H-mode discharges on DIII-D is the appearance of a series of small Type II ELMs leading up to a larger Type I ELM. The Type II ELMs become larger and fill the time interval between Type I ELMs, while the Type I ELM energy loss decreases, as the density is raised. In contrast to the results on ASDEX-Upgrade [19], the Type II ELMs on DIII-D do not completely replace the Type I ELMs in discharges without the RMP coil except at pedestal densities near the Greenwald density [22] where the pedestal pressure is strongly reduced. The Type II ELMs are more localized near the separatrix than the Type I ELMs as determined from profile reconstruction and soft x-ray observations, and have a

much larger ratio of midplane to divertor magnetic fluctuations. For the Type I ELMs the midplane magnetic signals often have a coherent structure which is consistent with the peeling-ballooning mode instability [20]. During the RMP coil on phase, in contrast to the Type I ELMs which remain relatively unchanged, the Type II ELMs appear to be enhanced (Fig. 7), appearing larger on edge soft x-ray signals and in magnetic fluctuations.

5.3. RMP H-mode at $\nu_e^* \sim 0.1$, $q_{95} \approx 7.5$, Odd RMP Coil Parity

With odd coil parity the resonant field is maximum at $q_{95} \approx 2.3$ and minimum at $q_{95} \approx 3.7$. There is a secondary maximum at $q_{95} \approx 7.5$ with RMP field about 3.6 times smaller than the primary maximum. By increasing the RMP coil current at $q_{95} \approx 7.5$, a resonant field amplitude about 80% of that required for ELM suppression at $q_{95} \approx 3.7$, was produced. In these $q_{95} \approx 7.5$ discharges, the pedestal pressure, J and p' were reduced nearly a factor of 2 compared to the no RMP case. In contrast to the $q_{95} \approx 3.7$ case, small ELMs with $\Delta W_{ELM}/W_{PED}$ reduced by more than a factor of 2 compared to the no RMP case persisted. These ELMs were a mixture of small and very small types suggesting the Type I ELM energy loss had decreased.

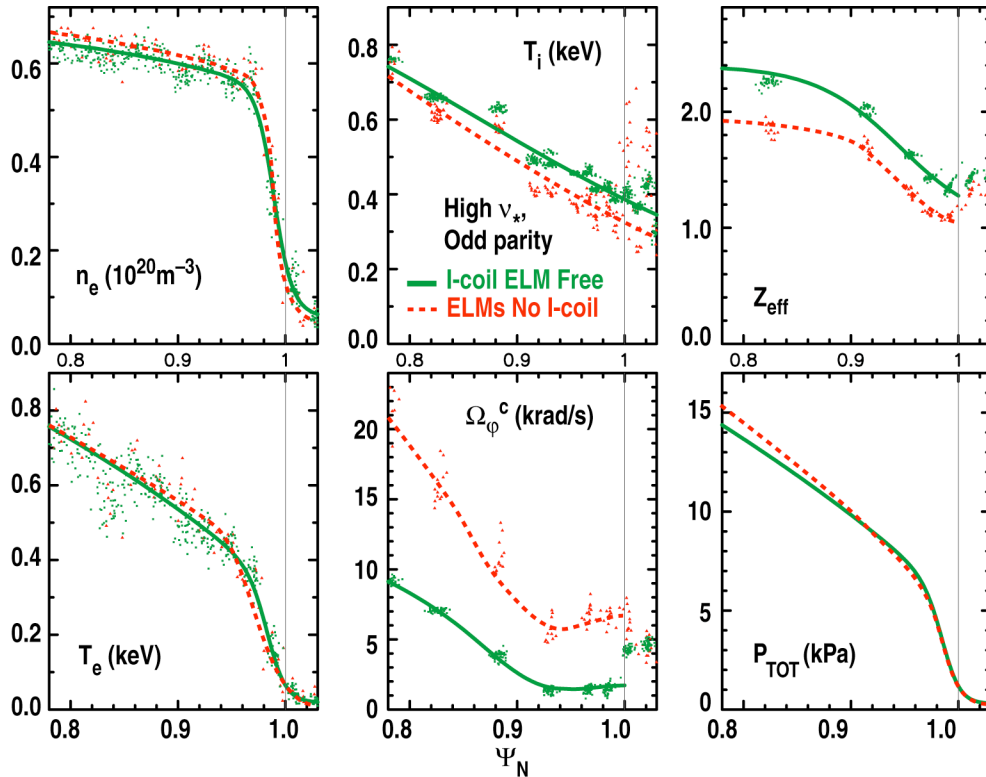


Fig. 6. Profiles near the ETB as a function of normalized poloidal flux, ψ_N , for $\nu_e^* \sim 1$, odd parity RMP ELM suppressed discharge (green) and just before a Type I ELM (red-dashed) with no RMP. The separatrix location is marked.

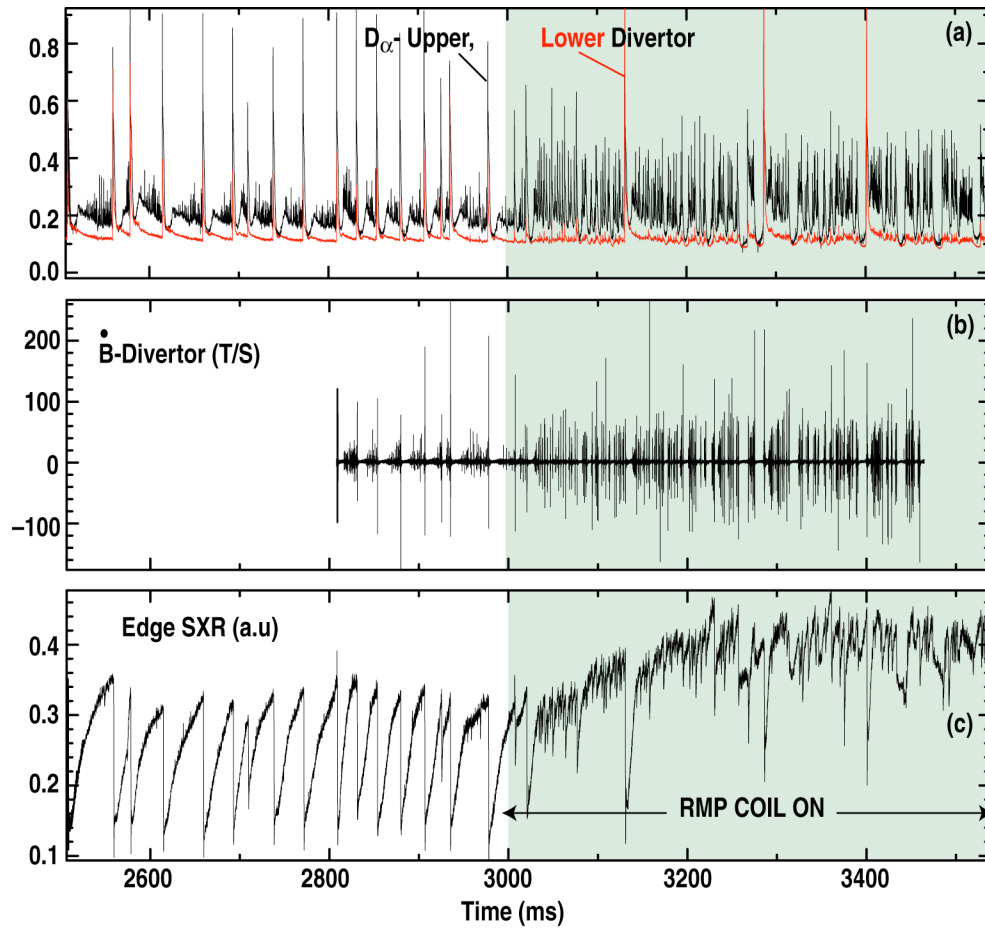


Fig. 7. The size of small, Type II, ELMs increase with RMP coil on in $\nu_e^* \sim 1$, odd RMP-coil parity discharge on (a) D_{α} , (b) magnetic probes in divertor region, and (c) edge SXR.

6. CONCLUSIONS

The hypothesis that QH-mode results from the saturation of a velocity shear driven low n peeling-ballooning mode is supported by several observations: 1) the mode number of the EHO, 2) the location of the QH-mode operating point near, but somewhat below the current limit for exciting an ELM, (measured from profiles and consistent with the current ramp experiment) 3) the low density requirement for QH-mode and the increase in that limit with strong plasma shaping, 4) the operational requirement of counter-injection where the velocity shear is inherently higher, and the loss of QH-mode as velocity shear is reduced with more balanced beam, 5) the damping of rotational shear when the EHO is present, 6) and the loss of QH-mode with plasma wall distance larger than a threshold value. On the basis of these results the possibility of obtaining QH-mode in ITER was investigated. Access to the low n peeling unstable regime in the ITER base case scenario would require $n_e^{PED} \leq 0.4 \times 10^{20} \text{ m}^{-3}$ [16]. This value is well below what is required to produce the desired fusion power output, $n_e^{PED} \approx 0.9 \times 10^{20} \text{ m}^{-3}$, however, it is possible that stronger shaping would allow access to this regime at higher density in ITER as it did in DIII-D. Neutral beams in ITER will be used for current drive as well as heating and therefore are to be oriented in the co-current direction. Our results do not rule out the possibility of QH-mode with only co-NBI given sufficient rotational shear.

The ability of the relatively simple RMP coil set to suppress Type I ELMs while maintaining good energy confinement is a positive result for future tokamaks. At ITER relevant collisionality, $\nu_e^* \sim 0.1$, the pedestal pressure was controlled and maintained below the peeling-ballooning mode stability limit while providing enough particle transport to avoid density or impurity accumulation. The control of pedestal pressure obtained in the low collisionality, even parity discharges may be a direct result of transport produced by the field stochastization. However, if this were the case it is not obvious why the strongest effect would be on the density profile since parallel transport should strongly affect the temperature.

In the case of ELM suppression a $\nu_e^* \sim 0.1$, where the part of the RMP coil field resonant with the equilibrium is small, the evidence suggests an indirect effect through the ELM instability. The Type II ELMs, which appear to be enhanced with the RMP coil on, may provide enough transport to avoid reaching the stability limit for the Type I. However, from this point of view, it is difficult to understand the fact that the pedestal pressure profile is quite similar in discharges where the Type I ELMs were completely suppressed compared to the pressure profile just before a Type I ELM with the RMP coil off. No evidence was found suggesting that the peeling-ballooning mode associated with the Type I ELM was transformed into a continuous instability. No such continuous instability was observed, while very similar rapidly growing MHD activity was seen on the outboard midplane probes before

a Type I ELM, and the Type I ELM was associated with about the same energy loss, with the RMP coil on and off. These results suggest that the Type II ELM has a very similar pressure gradient limit to the Type I and therefore is also likely the result of the peeling-ballooning instability but that for some reason the nonlinear phase of the instability is weaker or access to a transport channel is reduced. The Type II ELMs, or the RMP coil directly, might alter a feature other than the pressure profile which is critical for triggering large non-linear growth of the peeling-ballooning mode. It is possible that there is a difference in the pedestal current density with the RMP coil on and off, since this was not directly measured and is known to play a role in the peeling-ballooning stability. Changes in the rotation speed with the RMP coil on can be ruled out as altering the ELM instability since the Type I ELMs disappear before the rotation changes [21].

REFERENCES

- [1] Wilson H R, Cowley S C, Kirk A, and Snyder P B 2006 *Plasma Phys Control Fusion* **48** A71
- [2] Snyder P B et al 2004 *Plasma Phys Control Fusion* **46** A131
- [3] Ferron J R et al 2000 *Phys Plasmas* **7** 1976
- [4] Huysmans G T A 2005 *Plasma Phys Control Fusion* **47** B165
- [5] Sauter O, Angioni C, and Lin-Liu Y R 1999 *Phys Plasmas* **6** 2834
- [6] Osborne T H et al 2000 *Plasma Phys Control Fusion* **42** A175
- [7] Burrell K H et al 2002 *Fusion* **44** A253
- [8] Evans T E et al 2005 *Nucl Fusion* **45** 595
- [9] St John H E et al 1994 *Proc. 15th Intl Confe on Plasma Physics and Controlled Nuclear Fusion Research Seville (IAEA Vienna, 1995)* IAEA-CN-60/D-P22 603
- [10] Porter G D, Moller J, Brown M, and Lasnier C 1998 *Phys Plasmas* **5** 1410
- [11] Lao L L et al 2005 *Fusion Sci. Technol.* **48** 968
- [12] Thomas D M et al 2004 *Phys Rev Lett* **93** 065003
- [13] Wilson H R, Snyder P B, Huysmans G T A, Miller R L 2002 *Phys Plasmas* **9** 1277
- [14] Burrell K H et al 2005 *Phys Plasmas* **12** 056121
- [15] West W P et al 2005 *Nucl Fusion* **45** 1708
- [16] Snyder P B et al 2006 *Proc. 21st Intl Conf on Plasma Physics and Controlled Nuclear Fusion Research (Chengdu)* (IAEA Vienna) Paper TH/4-1Ra
- [17] Burrell K H et al 2004 *Plasma Phys Control Fusion* **46** A165
- [18] Evans T E et al 2006 *Nature Physics* **2** 419
- [19] Stober J et al 2001 *Nucl Fusion* **41** 1123
- [20] Perez C P et al 2004 *Nucl. Fusion* **44** 609
- [21] Evans T E et al 2004 *Phys Rev Lett* **92** 235003-1
- [22] Greenwald M et al 1988 *Nucl Fusion* **28** 2199

ACKNOWLEDGMENT

This work was supported by the U.S. Department of Energy under DE-FC02-04ER54698, W-7405-ENG-48, and DE-FG02-04ER54758.